

Impedance Studies of the Thin Film LiMn₂O₄ / Electrolyte Interface

K.A. Striebel^{*#}, E. Sakai^{*+} and E.J. Cairns^{*}
Environmental Energy Technologies Division
Ernest Orlando Lawrence Berkeley National Laboratory,
Berkeley, California 94720 USA

Abstract

Room-temperature impedance measurements of a thin-film LiMn₂O₄/LiPF₆-EC-DMC interface have been used to identify the spontaneous formation Li₂Mn₂O₄ at the interface at room temperature at voltages of 3.7 and higher. The impedance of the LiMn₂O₄ films exhibited two time constants: at about 14 kHz and 60 to 200 Hz. The high frequency loop is dependent on film morphology and was attributed to the substrate/oxide interface. The low frequency behavior was dependent on both state-of-charge (SOC) and time at a given SOC. At full charge the impedance in this electrolyte was stable at room temperature over several days. At high lithium contents, film OCV and impedance tended to grow logarithmically with time, with lower rates for lower Mn³⁺ content in the film. The increased impedance was removed by oxidation of the film to 4.5 V vs. Li/Li⁺. The observations are consistent with a reversible disproportionation of part of the LiMn₂O₄ into Li₂Mn₂O₄ and a lithium-deficient spinel. With extended constant current cycling part of the Li₂Mn₂O₄ degrades to the Mn₂O₃ and the process is no longer reversible.

* Electrochemical Society Active members

author to whom correspondence should be addressed: kastriebel@lbl.gov

+ present address: Sojo University, Kuamoto, Japan.

Introduction

The stability of the interface between LiMn_2O_4 and LiPF_6 -containing carbonate electrolytes, especially at elevated temperature, is critical to the commercial application of this otherwise desirable battery chemistry. Cell performance degrades at unacceptably high rates when LiMn_2O_4 electrodes are cycled against either lithium metal^{1,2} or carbon anodes^{3,4}, at temperatures of 50-60°C. The mechanisms proposed for the degradation vary widely and are discussed in depth in the recent paper by Amatucci et. al⁵. Most authors claim involvement by protons generated at the cathode by decomposition of the LiPF_6 -containing electrolyte^{2-4,6}, however reaction with pure DMC has also been shown to be detrimental⁷. In addition, the carbon used as an electronic conductor within the LiMn_2O_4 positive has been implicated in the degradation⁸. Acidic protons are clearly detrimental to a carbon anode, but they also appear in mechanisms for LiMn_2O_4 degradation through exchange for lithium in the structure and disproportionation of the Mn^{3+} followed by dissolution of Mn^{2+} from the cathode. The potential dependence of the degradation is also subject to uncertainty. It is clear that electrolyte oxidation will be more of a problem under fully charged (EOC) conditions, whereas disproportionation and distortion resulting from the presence of Mn^{3+} in the LiMn_2O_4 will occur more readily under fully discharged conditions (EOD). It has been known for a long time that discharge into the 3-volt region (insertion of lithium into LiMn_2O_4) leads to the formation of the $\text{Li}_2\text{Mn}_2\text{O}_4$ phase through the cooperative Jahn-Teller distortion⁹ and that this process leads to rapid capacity loss for the spinel¹⁰. It has also been proposed that non-equilibrium formation of $\text{Li}_2\text{Mn}_2\text{O}_4$ could occur under conditions of rapid discharge caused by local concentrations of Mn^{3+} high enough to cause the cooperative distortion¹¹. Thackeray et al. presented the first direct observation, with ex-situ TEM, of $\text{Li}_2\text{Mn}_2\text{O}_4$ at the surface of $\text{Li}_{1+y}\text{Mn}_{2-y}\text{O}_4$ grains that were cycled to voltages no lower than 3.5 V¹² at room temperature. This mechanism should be independent of the electrolyte, though this was not discussed in their work.

What is clear is that the degradation of LiMn_2O_4 is complex and occurs at least initially at the oxide/electrolyte interface. We have been using thin dense films of LiMn_2O_4 , produced with pulsed laser deposition (PLD), as a model system for the study

of the electrochemical properties of this important cathode material^{13,14} in the absence of conductive diluents or binders. In this work, this interface is studied with electrochemical impedance spectroscopy (EIS) at room temperature. The dependence of the impedance response on film morphology, film state-of-charge (SOC), the time spent at different SOC's yields interesting information regarding the initial steps in the mechanism for LiMn_2O_4 surface degradation. The progression of these steps during constant current cycling was also followed with EIS.

Experimental Procedures

Pure LiMn_2O_4 films are crystalline as prepared by pulsed laser deposition (PLD), at 600° C and 100 mtorr O_2 , on polished (0.1 μm) 0.3 cm^2 -diameter stainless steel substrates. Their structure, morphology and electrochemical behavior have already been reported^{14,15}. Ex situ Raman spectra were recorded using a Raman microscope by ISA Groupe Horiba, model Labram. The incident laser beam ($\lambda=632.8$ nm) was focused to 1.5 micron, and its power measured at the sample was adjusted to 10 mW, unless otherwise stated. Film morphology was evaluated with both atomic force microscopy (AFM) and optical interferometry (Zygo Microscope). Some films were deposited on a 100nm-thick Pt buffer layer, also prepared with PLD. "Powder" films were prepared as a porous PVdF-bonded $\text{Li}_{1.05}\text{Mn}_{1.95}\text{O}_4$ (obtained from EM Science) layer containing 5 wt% acetylene black on the same 0.3 cm^2 stainless steel disk. Films were studied by embedding the 3 mm disk into the end of a polypropylene or Kel-F rod, which was inserted into a polypropylene cell, fitted with lithium metal reference and counter electrodes and filled with about 5 ml of 1M $\text{LiPF}_6/\text{EC}/\text{DMC}$ (1:2) electrolyte (EM Science). Cyclic voltammetry (1 mV/s), used for film characterization, was carried out with a PAR 273 potentiostat. Electrochemical Impedance Spectroscopic (EIS) measurements were carried out with a Solartron 1260 FRA and a Solartron 1286 potentiostat using a perturbation of $\pm 10\text{mV}$ between 80k and 60mHz controlled by the ZPlot software. EIS data were fit to various circuit models with the ZView software.

Results and Discussion

Film Characterization

The LiMn_2O_4 films were crystalline as prepared (see Fig. 1) with lattice parameters very near 8.24 \AA , suggesting that they are close to stoichiometric. The lithium content was not measured directly due to the small chemical inventory of the PLD films. Film structure was also characterized with slow-sweep cyclic voltammetry (CV) and Raman spectroscopy. Fig. 2 shows the CV's recorded for three series of films, including one with a Pt buffer layer. The positions of the CV peaks shifted slightly between deposition runs but were quite consistent for films from the same run. The relative capacities (peak areas) of the lower to higher potential "4-volt" peaks can be used as a measure of the stoichiometry of the film¹⁴. Most of the films studied here showed peak ratios of about 52/47. One series of films had somewhat higher lithium content with a peak capacity ratio of about 58/42. These films showed slightly different impedance behavior, as will be discussed below. CV was also used to determine capacity, and film thickness was estimated using the theoretical density of 4.4 g/cm^3 . The films reported here had capacity densities of $12\text{-}15 \text{ }\mu\text{Ah/cm}^2$ and were nominally $0.3 \text{ }\mu\text{m}$ thick. The films prepared on the Pt buffer layer were found to be significantly smoother (about 6 times) than those without the buffer layer with both AFM and interferometric microscopy. The morphology of films deposited on the Pt buffer closely resembled that of the polished stainless steel substrate. Raman spectra for a fresh film and a $\text{Li}_{1.05}\text{Mn}_{1.95}\text{O}_4$ powder are compared in Fig. 3. Both show a strong peak at about 625 cm^{-1} and a shoulder at about 570 cm^{-1} , consistent with the literature¹⁶. There is some evidence of the four higher frequency peaks predicted by factor group theory.

In general, the LiMn_2O_4 films prepared in our lab show electrochemical behavior similar to those of bulk powders, however without the need for binders or conductive diluents. However, they tend to show somewhat better cycling stability especially at voltages outside the 3.7 to 4.35 voltage range usually employed for this material. This was clearly demonstrated in previous work, in the stability of films cycled between 2 and

5V vs. Li/Li^{+14} . None of the $\text{Li}_{1+y}\text{Mn}_{2-y}\text{O}_4$ films prepared with PLD in our laboratory have show the 3.3/4.5V redox peaks associated with the double-hexagonal structure.

General Impedance Behavior: Stainless Steel/ $\text{Li}_{1+y}\text{Mn}_{2-y}\text{O}_4$ /Electrolyte

The general impedance behavior of the stainless steel/ LiMn_2O_4 /electrolyte system was studied under a variety of conditions at room temperature. Slow sweep cyclic voltammetry (1 mV/sec) was used to bring films to a specific state-of-charge (SOC). The potential was then allowed to "rest" for 15 minutes and then the impedance spectrum was measured. Figure 4 shows the Nyquist plot for a fresh LiMn_2O_4 film in LiPF_6 -electrolyte at end-of-charge (EOC) and end-of-discharge (EOD), or at about 4.2 and 3.9 V vs. Li/Li^+ , respectively. The general features observed for all of the PLD-deposited films are a high-frequency loop from 80 kHz to about 3000 Hz ($1/\tau_1 = 14\text{kHz}$), a mid-frequency loop ($1/\tau_2 = 60\text{-}200$ Hz) and a low frequency arm that in some cases extends to pure capacitive behavior. The high-frequency loop was generally stable for all states-of-charge (SOC), whereas the mid to low frequency behavior was found to depend on SOC, and time in the electrolyte.

Morphology Dependence at High Frequency

The high frequency limit is characterized by an ohmic resistance for this cell that varies from about 25 to 50 Ω depending on the exact position of the WE shaft relative to the RE. This is consistent with an electrolyte conductivity of about 10 $(\Omega\text{cm})^{-1}$. The high frequency loop is often attributed to the growth of a surface film on an electrode. The shape and size of this loop was fairly independent of film SOC, time in the electrolyte or cycling history, except when a film separated from the substrate surface. All of these characteristics are consistent with an interface more removed from the electrolyte, such as the LiMn_2O_4 / substrate interface. To investigate this further, the high-frequency parts of the spectra for three films of varying morphology are compared in Fig. 5. The data are shown for EOC and EOD conditions in the same electrolyte. The films shown, in order of increasing roughness, are PLD- LiMn_2O_4 / Pt / stainless steel < PLD- LiMn_2O_4 / stainless

steel < "powder LiMnO₄ film" / stainless steel. Qualitatively, the size of this high frequency loop **decreases** with **increasing** interfacial surface area. The high frequency behavior can be fit with a resistor (R_Ω) in series with a parallel combination of a constant phase element (CPE_S) and another resistor (R_S). The CPE is often used to model a porous electrode where it is used as an approximation of the transmission line circuit. This approach has been used to characterize surface roughness in electrochemical systems¹⁷. Table 1 shows the parameters derived from fitting the data in Figure 5. The capacitance of this interface was estimated from the impedance at 10k Hz and the angle ϕ characterizes the depression of the semicircle below the real axis. As mentioned above, the addition of a Pt buffer layer to the stainless steel surface reduces the roughness of the LiMn₂O₄ deposited on top of it by a factor of about 6. The increase in roughness for the "porous" electrode was estimated from the difference in the active material loading, or about 65 times. The increase in the capacitance of this interface with roughness makes sense. The increase in ϕ with roughness for the PLD films is also consistent with the literature¹⁷. The varying resistance, R_S , could certainly be influenced by the presence of carbon in the "powder" film and an effect of the Pt buffer layer.

Reversible Impedance Changes with Time

Initial spectra recorded for films taken to EOD were scattered widely because the time between the CV and impedance measurements was not carefully controlled. The time dependence was characterized by utilizing the batch mode of the ZPlot control program. EIS data were recorded at preset intervals from 1 to 2000 minutes at a given SOC. The film was at open circuit in between measurements. Figure 6 shows Nyquist plots of the impedance at a series of times recorded at EOD and EOC. The first few measurements, at time < 15 minutes, reflect changes due to the relaxation of the Li concentration gradient resulting from the potential sweep experiment and these are omitted from Fig. 6 for clarity. At times greater than 15 minutes, both the impedance response and film voltage at EOC are remarkably stable with time. However, at higher lithium contents both the film potential and the size of the mid-frequency loop increase logarithmically with time.

The size of this loop is controlled primarily by the charge-transfer kinetics at the interface. For simplicity in analysis we are using the magnitude of the impedance, at a fixed frequency, to quantify the changes with time, as illustrated in Figure 7 for two states-of-charge. It is clear that the rate of the impedance rise decreases with an increase in the SOC, or decrease in the amount of Mn^{3+} in the film. The one lithium-excess film studied with this technique also showed a rise in impedance with time but with a somewhat delayed response (also shown in Fig. 7). This film is expected to have a lower initial Mn^{3+} content.

The spontaneous impedance rises measured at EOD were found to be **reversible** for all films tested. After measuring the 1080-minute spectrum (Fig.6), the potential was swept at 1 mV/s for 4 cycles between 3.7 and 4.5 V vs. Li/Li^+ , again ending at 3.7V. The "recovered" impedance (see Fig.6), recorded after a 15 min. rest period, can be seen to be almost identical to the prior trace. The first anodic sweep of this recovery CV (shown in Figure 8) shows that the energetics of the film have changed significantly during the time spent at EOD. The anodic peaks tend to shift to higher potential and collapse into one peak. This behavior is characteristic of an increased resistance and possibly a disordering of the Li ions in the oxide film¹³. The charge passed during the first anodic sweep is only slightly higher than succeeding cycles, probably not indicative of a faradaic oxidation of this "layer". No capacity fade of the LiMn_2O_4 film was recorded after the one-day hold at open circuit for either charged or discharged films, suggesting that neither Mn nor Li was lost during this experiment. The distorted CV from Fig. 8 is compared in Fig. 9 with the CV recorded on a film held for one hour at 3.5 volts and one that was swept to a voltage of 2.0 V vs. Li/Li^+ . All of these distorted CV's reverted to the classic shape after a few cycles between 3.7 and 4.5 vs. Li/Li^+ .

Voltage rises at EOD have been observed previously with thin film electrodes¹⁸ at elevated temperatures and have been attributed to a disproportionation ($2\text{Mn}^{3+} \rightarrow \text{Mn}^{2+} + \text{Mn}^{4+}$) followed by Mn^{2+} dissolution in $\text{LiPF}_6/\text{carbonate}$ electrolytes, leaving the higher voltage $\lambda\text{-MnO}_2$. However, this process is not reversible and the degradation of the LiMn_2O_4 will result. Recently, SEI layers containing Li_2O or lithium alkoxides have been observed directly by Raman spectroscopy of films held at elevated temperatures in these electrolytes at elevated temperatures⁷. We believe that we are observing an initial step in

this process. At room temperature the disproportionation reaction proceeds as far as the formation of $\text{Li}_2\text{Mn}_2\text{O}_4$ on the surface according to the reaction



leaving a bulk film with a slight lithium deficiency. $\text{Li}_2\text{Mn}_2\text{O}_4$ is known to be an insulator, and have poor kinetics for lithium exchange. The lithium-deficient portion of the film would cause the observed increase in the open-circuit voltage of the film. In addition, $\text{Li}_2\text{Mn}_2\text{O}_4$ is expected to be oxidized upon cycling to 4.5 V vs. Li/Li^+ . All of these observations are consistent with the formation of $\text{Li}_2\text{Mn}_2\text{O}_4$ at the surface.

It could be argued that $\text{Li}_2\text{Mn}_2\text{O}_4$ is not expected to be present at potentials above 3 V vs. Li/Li^+ . However, a finite amount of tetragonal spinel has been identified in ex-situ TEM measurements on the surface of grains of $\text{Li}_{1+y}\text{Mn}_{2-y}\text{O}_4$ cycled to potentials 3.0, 3.3 and 3.5V^{12,19}. Extrapolation of their results to the minimum voltage of 3.7 V used in the present study reveals that a finite amount could be expected there as well. The formation of the lower voltage phase during high-rate cycling was attributed to localized non-uniformities in the $\text{Mn}^{3+}/\text{Mn}^{4+}$ distribution. At any point where the local concentration of Mn^{3+} exceeds 50%, there will be a tendency for the spinel to distort¹¹. A slight excess of Mn^{3+} might be expected at the surface of a film (or grain) because of the lower constraints on the crystal and volume considerations, since the distorted spinel requires a larger volume than the cubic spinel.

Further evidence of $\text{Li}_2\text{Mn}_2\text{O}_4$ can be seen from CV and Raman measurements. Fig. 9 shows similar shapes of the oxidation peaks for the film left at EOD with those for a film that had been previously reduced well into the tetragonal phase region with CV. These peaks were explained as the slow removal of Li^+ from the octahedral sites that are populated in the tetragonally distorted spinel¹³. In Fig. 10, Raman spectra recorded for films that were left in the electrolyte at room temperature and EOD, for 18h and 2 weeks are compared with spectra for a fresh film and a chemically-prepared $\text{Li}_2\text{Mn}_2\text{O}_4$ powder reference. The 18h film shows a strong peak at about 605 cm^{-1} that is clearly attributable to the tetragonal spinel, with shoulders on either side from the remaining cubic phase. The spectrum for the film left at EOD for 2 weeks shows the 605 cm^{-1} peak as well as a

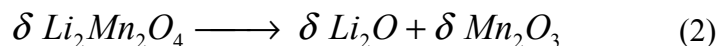
large peak at about 660 cm^{-1} , which is characteristic of another manganese oxide such as Mn_2O_3 ^{7,16}. This last spectrum suggests that the impedance rise with time characterized by equation 1 is a preliminary step in the degradation process for the spinel. Further degradation then proceeds to the formation of the Mn_2O_3 and the process is no longer reversible. No evidence of disproportionation of $\text{Li}_2\text{Mn}_2\text{O}_4$ into the rocksalt phase Li_2MnO_3 was observed.

It should be noted that only very small increases in the impedance of the "powder film" electrode with time were observed at any state-of-charge. There are a number of possible explanations for this observation. Most probable is the significantly higher volume to surface area ratio for this "film". In addition the porous film contains carbon that is present with 10 times the surface area of the oxide. The impedance response of a pure carbon electrode in this potential range was not measured. It has been suggested that carbon present with the oxide is acting to prevent the formation of the surface layer²⁰. Some studies have been carried out with PLD-prepared LiMn_2O_4 film to which a partial coating of evaporated carbon has been added. However, impedance rises similar to those discussed here were usually recorded for these carbon-coated films.

Cycling Studies

EIS was also investigated as a tool to examine changes in the behavior of LiMn_2O_4 films with constant-current cycling. The rate of the formation of the $\text{Li}_2\text{Mn}_2\text{O}_4$ layer on the film with time was the same before and after cycling (also shown in Fig. 7) however the starting impedance was clearly higher after cycling. To gain insight into the changes occurring within the film as well as at the interface during cycling, cyclic voltammograms and impedance spectra as a function of state-of-charge were measured at different points during the cycling. Films were cycled at $\pm 35\text{ }\mu\text{A}/\text{cm}^2$ (about 2.3C) between 3.7 and 4.35 V. Initially the films were allowed to rest for 15 min. at open circuit between half cycles (regimen A). However, because of the large impedance increases at EOD discussed above, the cycling regimen was modified to include only 15 s rest periods (regimen B). In general, the change in cycling protocol did not improve the capacity retention with cycling. However, different mechanisms for the degradation are evident

from the shape of the CV's recorded during cycling. Figure 11 shows CV's recorded before and after cycling with the two regimens. In both cases the loss in capacity was about 12% but the shapes of the CV's were quite different. For regimen B, the CV suggests that the film thickness is simply decreased with cycling. For regimen A, with significant time spent at EOD during the cycling (18% of each cycle) the current signal is more dispersed in voltage and the separation between the anodic and cathodic peaks is increased. This behavior is characteristic of an increase in the film porosity and the formation of a resistive layer, respectively. After the extended periods at EOD experienced by the films cycled with regimen A, the next step in the degradation could be occurring, namely decomposition of the $\text{Li}_2\text{Mn}_2\text{O}_4$ into other Mn^{3+} oxides with the simultaneous loss of Li and/or O to the electrolyte or to an SEI layer on the film.



We don't have direct evidence of this reaction from a cycled film, however the film left at EOD for 2 weeks did show Raman peaks characteristic of Mn_2O_3 as was shown in Fig. 10. This step has been proposed as a possible pathway for the degradation of $\text{Li}_2\text{Mn}_2\text{O}_4$. It was suggested that in acidic electrolytes the Mn_2O_3 will be subject to disproportionation and the reaction products would instead be MnO and Li_2MnO_3 ²¹. However, the rocksalt phase was not observed in the Raman spectra, as discussed above. Reaction 2 may be stabilized by the formation of the SEI layer under these relatively mild electrolyte conditions.

Sample Nyquist plots for a LiMn_2O_4 film after 34 and 88 cycles with regimen B are shown in Fig. 12. Impedance changes with time, SOC and cycle history are manifested in the frequency range of 200 Hz to 60mHz. Several circuits were evaluated to find the best fit for these spectra along with those recorded at intermediate SOC's (not shown). The circuit shown in Fig. 13 represents the simplest circuit to provide an adequate fit. Spectra recorded for films cycled with regimen A are visibly the same as those in Fig. 12, however, the circuit model had to be modified by replacing the capacitor C_1 with an additional constant-phase element. The spectra were recorded by charging the film to a given SOC and then holding for 15 min at OC before making the measurement. The

measurements were automated with the Batch mode in the ZPlot software, allowing accurate reproduction of the experiment timing.

There are nine parameters that result from the six circuit elements in Fig.13, although the ohmic resistance, R_{Ω} , was constant. The interpretation of the parameters is complicated by the accumulation of impedance rises with time during the measurements from EOD to EOC. This is obvious from a comparison between the shapes of spectra recorded at EOC in Figs. 6 and 12. In Fig. 6 they were recorded as a function of time after a potential sweep to 4.5V with no appreciable time spent at other potentials. The changes in several of the parameters with SOC are shown in Fig. 14. Higher R_{ct} 's (Fig. 14A) were measured at all SOC's after longer cycling, however, the rate of increase with time didn't change much as was seen in Fig. 7. During cycling to an upper limit of only 4.35V, not all of the $Li_2Mn_2O_4$ formed during periods at EOD will be reoxidized. Even a thin layer of $Li_2Mn_2O_4$ on the film surface would be expected to reduce the kinetic activity of the surface. The Warburg element is used to characterize the diffusion process within the film; $W_T=L^2/D$ where L is the thickness of the film and D is the lithium diffusivity. The decrease in lithium diffusivity within $LiMn_2O_4$ as lithium content decreases (SOC increases), shown in Fig. 14B, is consistent with the results of Julien et. al¹⁶ and is explained by a decrease in the lattice parameter. The decrease in W_T with cycling could reflect a decrease in the film thickness. The CPE_p parameter is characteristic of the degree of inhomogeneity of the interface. A decrease in this parameter would be expected with an increase in film porosity with cycling as is seen in Fig. 14C.

Conclusions

Measurements of the impedance of the $LiMn_2O_4$ /electrolyte interface as a function of time, state-of-charge and cycling history has yielded new observations regarding the stability of this oxide in battery electrolytes. A spontaneous impedance rise with time at end-of-discharge conditions was measured and attributed to a reversible disproportionation reaction of part of the $LiMn_2O_4$ into $Li_2Mn_2O_4$ at the surface and a lithium-deficient material, $Li_{1.8}Mn_2O_4$ in the rest of the film. Results are consistent with

literature reports of the presence of $\text{Li}_2\text{Mn}_2\text{O}_4$ at this interface for cycled electrodes. Time spent at end-of-discharge conditions was found to affect the cycling behavior of the oxide and oxidation of films with a high impedance build-up was found to improve performance. The CV and EIS analysis of these films during cycling suggests that the formation of $\text{Li}_2\text{Mn}_2\text{O}_4$ at the surface is an initial step in the degradation of LiMn_2O_4 electrodes.

Acknowledgments

E. Sakai was a visiting scholar from the The Kuamoto Institute of Technology, Kuamoto, Japan. We would like to thank R. Reade for the preparation of the films, T. Richardson for discussions and R. Kostecki for the AFM and Raman measurements. This work was supported by the Office of Energy Research, Basic Energy Sciences, Chemical Sciences Division of the Department of Energy under contract No. DE-ACO3-76SF00098.

References

1. Y. Xia, Z. Zhou and M. Yoshio, This Journal **144**, 2593 (1997).
2. T. Inoue and M. Sano, This Journal **145**, 3704 (1998).
3. G. Amatucci, A. Du Pasquier, A. Blyr, T. Zheng and J-M. Tarascon, Electrochim. Acta **45**, 255 (1999).
4. E. Wang, D. Ofer, W. Bowden, N. Ilchev, R. Moses and K. Brandt This Journal **147**, 4023 (2000)
5. G. Amatucci, N. Pereira, T. Zheng and J-M. Tarascon, This Journal **148**, A171 (2001).
6. A. Blyr, C. Sigala, G. Amatucci, A. Du Pasquier, D. Guyomard, Y. Chabre and J-M. Tarascon, This Journal **145**, 194 (1998).
7. Y. Matsuo, R. Kostecki, F.R. McLarnon, This Journal **148**, A687 (2001).
8. D. H. Jang and S. M. Oh, Electrochim. Acta **43**, 1023 (1998).

9. M. Thackeray, W.I.F. David, P. G. Bruce and J. B. Goodenough, *Mater. Res. Bull.* **18**, 461 (1983).
10. M. M. Thackeray, *Prog. Solid State Chem.* **25**, 1 (1997).
11. R. J. Gummow, A. de Kock and M. M. Thackeray, *Sol. State Ionics* **69**, 59 (1994).
12. M.M. Thackeray, Y. Shao-Horn, A.J. Kahaian, K.D. Kepler, E. Skinner, J.T. Vaughey, and S.A. Hackney, *Electrochem. Sol. State Lett.* **1**, 7 (1998).
13. A. Rougier, K.A. Striebel, S.J. Wen, and E.J. Cairns, *J. Electrochem. Soc.*, **145**, 2975 (1998).
14. K.A. Striebel, A. Rougier, C.R. Horne, R.P Reade and E.J. Cairns, *J. Electrochem. Soc.* **146**, 4339 (1999).
15. A. Rougier, K.A. Striebel, S. J. Wen, T.J. Richardson R.P Reade and E.J. Cairns, *Appl. Surf. Sci.* **134**, 107 (1998).
16. C. Julien, E. Haro-Poniatowshi, M. A. Camacho-Lopez, L. Escobar-Alarcon, and J. Jimenez-Jarquin, *Mats. Sci. Engr.* **B72** (2000) 36.
17. U. Rammelt and G. Reinhard, *Electrochim. Acta* **35**, 1045 (1990).
18. T. Uchiyama, M. Nishizawa, T. Itoh and I. Uchida, *J. Electrochem. Soc.* **147**, 2057 (2000).
19. Y. Shao-Horn, S.A. Hackney, A.J. Kahaian, K.D. Kepler, E. Skinner, J.T. Vaughey, and M.M. Thackeray, *J. Power Sources* **81-82**, 496 (1998).
20. K.A. Striebel and E.J. Cairns, Extended Abstract 167, Joint Int'l Meeting, The Electrochem. Soc., Honolulu, HI, Oct. 1999.
21. J. Cho and M.M. Thackeray, *This Journal* **146**, 3577 (1999).

Table 1 Parameters from fit of high-frequency impedance of $\text{Li}_{1+y}\text{Mn}_{2-y}\text{O}_4$ films with different morphology.

System	Roughness Factor	SOC	R_Ω (Ω)	R_s (Ω)	C_s (μF)	ϕ ($^\circ$)
PLD- LiMn_2O_4 / Pt / stainless steel	1	EOD	29	263	0.48	17
		EOC	29	224	0.53	20
PLD- LiMn_2O_4 / stainless steel	6	EOD	35	83	0.71	30
		EOC	36	81	0.73	30
Porous LiMn_2O_4 / stainless steel	390	EOD	46	24	2.03	23
		EOC	45	33	1.39	18

Figure Captions

Fig. 1. Xray diffraction pattern for a $\text{Li}_{1+y}\text{Mn}_{2-y}\text{O}_4$ film on stainless steel.

Fig. 2. Cyclic voltammogram (1 mV/s) for two $\text{Li}_{1+y}\text{Mn}_{2-y}\text{O}_4$ films on stainless steel (- - - and — —) and one with a Pt buffer layer (—).

Fig. 3 Raman spectra of a typical PLD film, and $\text{Li}_{1.05}\text{Mn}_{1.95}\text{O}_4$ powder received from EM Science.

Fig. 4. Nyquist plots (80k to 60mHz) for a LiMn_2O_4 film on stainless steel in 1M $\text{LiPF}_6/\text{EC}/\text{DMC}$ (1:2) at 3.95V (EOD): - - - - and 4.21V (EOC): — — .

Fig. 5. High-frequency Nyquist plots for 3 LiMn_2O_4 electrodes with different morphologies at EOD (open symbols) and EOC (closed symbols): LiMn_2O_4 / Pt / SS: ☒, ☆; LiMn_2O_4 / SS: ρ, π; powder LiMn_2O_4 “film”/ SS: ☒, ☐.

Fig. 6 Time-dependent Nyquist plots for stoichiometric LiMn_2O_4 film on stainless steel in 1M $\text{LiPF}_6/\text{EC}/\text{DMC}$, 25°C.

Fig. 7. Time variation of total impedance $|Z|$ (open symbols) and OCV (closed symbols) for several LiMn_2O_4 films at different states-of-charge: stoichiometric film at EOD: ☒, ☐; stoichiometric film at MOD: ☒, ☆; lithium-excess film at EOD: ρπ; stoichiometric film at EOD after cycling: ♪.

Fig. 8. "Recovery" of original CV shape after holding LiMn_2O_4 film at EOD for 1080 min, — — original CV, — — after 1080 min. at EOD, - - - - “recovered” CV after 3 cycles between 4.5 and 3.7 V.

Fig. 9. Comparison of anodic peak voltages for different cathodic treatments: - - - - sweep down to 2 V, — — 1 h hold @ 3.5V, — — 18h hold at 3.7 V.

Fig. 10. Raman spectra for LiMn_2O_4 films: fresh, after overnight and after 2 weeks at EOD.

Fig. 11. Comparison of CV change with different cycling protocols: LiMn_2O_4 films before and after about 88 constant current ($\pm 35\mu\text{A}/\text{cm}^2$) cycles with 15 min. holds (A) and with 15s holds (B) at open circuit between half-cycles: — — fresh films, — — cycled films.

Fig. 12. Nyquist plots for a LiMn_2O_4 film at EOD (filled symbols) and EOC (open symbols), at 34 (■, ☆) and at 88 (□, □) cycles.

Fig. 13. Circuit for modeling impedance data from LiMn_2O_4 film on stainless steel.

Fig. 14 Model parameter dependence on state-of-charge at 34 cycles (■) and after 88 cycles (□) at room temperature: (A) R_{ct} , (B) W_T , (C) CPE_p .